Influence of neutrons and γ-rays in the Frejus underground laboratory on the NEMO experiment

Christine Marquet, F. Piquemal, R. Arnold, C. Augier, J. Baker, A. Barabash, O. Bing, D. Blum, V. Brudanin, J. Caffrey, et al.

Influence of neutrons and γ-rays in the Fréjus underground laboratory on the NEMO experiment

Ch. Marquet[a,*], F. Piquemal[a], R. Arnold[b], C. Augier[c], J. Baker[d], A. Barabash[e], O. Bing[b], D. Blum[c], V. Brudanin[f], J. Caffrey[d], J.E. Campagne[c], E. Caurier[b], D. Dassie[a], V. Egorov[f], K. Errahmane[c], R. Eschbach[a], T. Filipova[f], J.L. Guyonnet[b], C. Jollet[a], S. Jullian[c], F. Hubert[a], Ph. Hubert[a], I. Kisel[f], O. Kochetov[f], V.N. Kornoukhov[e], V. Kovalenko[f], D. Lalanne[c], F. Laplanche[c], F. Leccia[a], I. Linck[b], C. Longuemare[g], F. Mauger[g], H.W. Nicholson[h], I. Nikolic-Audit[a], H. Ohsumi[a], I. Pilugin[e], J.L. Reyss[i], X. Sarazin[c], F. Scheibling[b], I. Štekl[j], J. Suhonen[k], C.S. Sutton[h], G. Szklarz[c], V. Timkin[f], V. Tretyak[f], V. Umatov[e], L. Vála[j], I. Vanyushin[e], A. Vareille[a], V. Vorobel[l], Ts. Vylov[f]

NEMO collaboration

[a]*CENBG, IN2P3-CNRS et Université de Bordeaux I, 33175 Gradignan, France*
[b]*IReS, IN2P3-CNRS et Université Louis Pasteur, 67037 Strasbourg, France*
[c]*LAL, IN2P3-CNRS et Université de Paris-Sud, 91405 Orsay, France*
[d]*INEEL, Idaho Falls, ID 83415, USA*
[e]*ITEP, 117259 Moscow, Russia*
[f]*JINR, 141980 Dubna, Russia*
[g]*LPC, IN2P3-CNRS et Université de Caen, 14032 Caen, France*
[h]*MHC, South Hadley, MA 01075, USA*
[i]*LSCE, CNRS, 91190 Gif sur Yvette, France*
[j]*CTU FNSPE, Prague, Czech Republic*
[k]*Jyväskylä University, 40351 Jyväskylä, Finland*
[l]*Charles University, Prague, Czech Republic*

To be sensitive to an effective Majorana neutrino mass, $\langle m_\nu \rangle$, on the order of 0.1 eV, the NEMO 3 double beta ($\beta\beta(0\nu)$) decay experiment requires precise knowledge and control of the backgrounds. The effect of neutrons and γ-rays from the Fréjus underground laboratory (LSM, Laboratoire Souterrain de Modane) has been studied during 10 700 h of data collection. The data were taken with a NEMO 2 prototype detector using different shield configurations. Monte Carlo

* Correspondence address. IReS, 23 rue du Loess, 67037 Strasbourg, Cedex 2, France. Tel.: + 33-3-88-66-1065-81; fax: + 33-3-88-66-1062-64 .

E-mail address: christine.marquet@ires.in2p3.fr (Ch. Marquet).

calculations with GEANT/MICAP code and a new library of γ-rays from neutron captures are presented. The implied consequences for the NEMO 3 detector which is under construction are discussed. The neutrinoless double beta decay background induced by neutrons and γ-rays within the LSM will be suppressed to the very suitable level of 0.1 event in a live time of five years given the appropriate shield and magnetic field.

Keywords: Neutron; γ-ray; Monte Carlo simulation; Background; Double-beta decay

1. Introduction

Neutrinoless double beta decay ($\beta\beta(0\nu)$) is a test of physics beyond the Standard Model of electroweak interactions by invoking a new physics: non-conservation of lepton number, existence of massive Majorana neutrinos, right-handed currents and massless Goldstone bosons (Majoron) [1]. The observation of $\beta\beta(0\nu)$ decay is the only way to prove the existence of massive Majorana neutrinos. Given the neutrino oscillation evidence, the energy domain below 1.0 eV for the effective neutrino mass ($\langle m_\nu \rangle$) is of particular interest for models involving hierarchy mass and phenomenologically viable four-neutrinos scenarios [2].

Since 1989 the Neutrinoless Experiment with Molybdenum (NEMO) collaboration has worked on a research and development program to build a detector capable of reaching an effective neutrino mass of 0.1 eV. The $\beta\beta(0\nu)$ (0^+ g.s. $\rightarrow 0^+$ g.s.) signal consists of two emitted electrons with their summed energy equal to the available energy, $Q_{\beta\beta}$. The NEMO experiment is based on the direct detection of these electrons by a tracking device and on the measurement of their energies by a calorimeter. The expected half-lives of $\beta\beta(0\nu)$ decay are very long (greater than 10^{24} years) and $Q_{\beta\beta}$ is a few MeV ($Q_{\beta\beta} = 3.034$ MeV for ^{100}Mo). All the contributing backgrounds which are relevant must be minimized. This implies the installation of the detector in an underground laboratory, use of γ-ray and neutron shields and very careful selection of radiopure materials.

To study the technical feasibility, as well as the different backgrounds in the 3 MeV energy range, two prototypes have been built (NEMO 1 [3] and NEMO 2 [4]). They ran from 1991 to 1997. In this paper the tests performed with the NEMO 2 prototype on γ-ray and neutron backgrounds with several kinds of shields and neutron sources are reported. A comparison of data is made with the simulations performed with the GEANT/MICAP code improved for the specific γ-ray emission. Finally, the insights of this study are presented in the context of the NEMO 3 detector [5] which is under construction in the LSM.

2. Neutron and γ-ray environment in the LSM

2.1. Origins of the neutrons

In all underground laboratories the known sources of neutrons are due to (α,n) reactions, spontaneous fission of uranium and the interaction of cosmic ray muons [6] in the rocks.

In the LSM, taking into account the activities of the rock and concrete, (α,n) reactions and spontaneous fission of uranium contribute equally to the neutron flux [7]. At the depth of the LSM (4800 m.w.e.) the measured muon flux is 5×10^{-9} s^{-1} cm^{-2}. This flux is lower by a factor of 2×10^6 than the flux at sea level [8]). Thus, the neutron production by muons is negligible compared to the other sources. The measured thermal ($\simeq 0.025$ eV) and fast (> 1 MeV) neutron fluxes are $(1.6 \pm 0.1)10^{-6}$ s^{-1} cm^{-2} and (4.0 ± 1.0) 10^{-6} s^{-1} cm^{-2}, respectively [7]. For intermediate energies there has been no measurement in the LSM but the measurements realized in different underground laboratories (Gran Sasso 3900 m.w.e. [6] and Broken Hill 3200 m.w.e. [9]) have shown that the epithermal neutron flux is on the same order of magnitude as the thermal neutron flux. The same is assumed for the LSM.

2.2. Origins of the γ-rays

Gamma ray fluxes are currently measured with a low-background NaI detector in the LSM. Depending on the energy domain, the γ-rays come from the natural radioactivity in the surrounding rock, radiative neutron capture and muon bremsstrahlung.

The natural radioactivity contributes events mostly up to 2.6 MeV which corresponds to the γ-ray transition of ^{208}Tl. Above this energy and up to 10 MeV the main source of γ-rays is neutron captures in the surrounding materials. Beyond 10 MeV only bremsstrahlung of muons contributes.

Preliminary results [10] gave an estimate of the fluxes at $(3.2 \pm 1.1)10^{-6}$ s^{-1} cm^{-2} for γ-rays in the 6–10 MeV energy domain and $(1.0 \pm 0.3)10^{-8}$ s^{-1} cm^{-2} for γ-rays with energies greater than 10 MeV. The flux between 3 and 6 MeV has been estimated with the NaI detector taking into account its internal background from α and β activities. This flux is similar to the one in the 6–10 MeV domain.

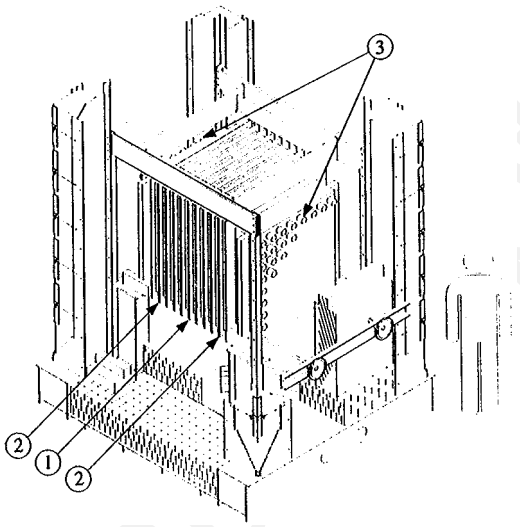

Fig. 1. The NEMO 2 prototype without shield. (1) Central frame with the source plane capable of supporting plural source foils. (2) Tracking device of 10 frames, each consisting of two perpendicular planes of 32 Geiger cells. (3) Two scintillator arrays first with 8×8 counters each and then with 5×5 counters each (in this paper only the results recorded with 5×5 configuration are used).

3. The NEMO 2 experiment

3.1. The NEMO 2 prototype detector

Only the pertinent characteristics of the detector will be presented here. A more detailed description can be found in Ref. [4]. The NEMO 2 detector (Fig. 1) consisted of a 1 m^2 source foil of 50 mg cm^{-2} thick placed between two tracking volumes composed of drift-Geiger cells and a calorimeter of two plastic scintillator arrays. In order to minimize multiple scattering effects, the tracking volumes were filled with a mixture of helium gas and 4% ethyl alcohol. The detector was able to track electrons with energies as low as 100 keV and a trigger allowed NEMO 2 to detect delayed α particles for background studies. The calorimeter was made of two arrays of 25 plastic scintillators coupled to low-activity photomultiplier tubes (PMT). These counters allowed energy and time-of-flight measurements. The resolution was 17.4% (FWHM) in energy and 250 ps (1σ) in time at 1 MeV. The detection threshold was set at 50 keV and the maximum measured energy for each element of the calorimeter was on the order of 4 MeV. A laser system daily checked on time and energy calibrations, and periodically measured the linearity of the calorimeter response. The mechanical frame of the detector was made of very low radioactivity (OFHC) copper. Finally, the detector was surrounded by an external shield for which the configuration was changed several times to understand the external background. For each configuration a minimum of 20 cm of iron was present.

3.2. Selection of ββ events

The detector was able to distinguish between charged particles and γ-rays. An electron's (or positron's) signature was a track linking the foil to a fired scintillator with a maximum scattering angle of less than 20° to avoid hard scattering. A photon corresponded to one or several adjacent fired scintillators without an associated track.

A ββ decay candidate, called a "two-electron" event, was characterized by two tracks each linked

to fired scintillators with a common vertex on the foil. A time-of-flight (TOF) measurement and subsequent cut allowed NEMO 2 to distinguish between two electrons emitted from the foil and one electron crossing the detector. To insure a precise TOF cut, a 200 keV threshold was applied to the energy deposited in the plastic scintillators for both electrons and photons. Methods used to calculate the time differences are detailed in Ref. [11].

3.3. *Background of the* ββ(0ν) *decay*

In the NEMO experiment, a signal from ββ(0ν) decay for ^{100}Mo is expected to be between 2.8 and 3.2 MeV. This energy range is determined by the energy resolution of the calorimeter and the energy losses inside the source foil and the wire chamber. Several sources of background can occur in this energy domain. They are classified as "external" or "internal" depending on their origin.

The "internal" background comes from the beta decay of emitters such as the isotopes ^{214}Bi ($Q_\beta = 3.2$ MeV) and ^{208}Tl ($Q_\beta = 5.0$ MeV) which are present in the source. They can mimic ββ events by β emission followed by Möller effect or by β–γ cascade followed by a Compton interaction. Detailed studies of this background have already been published in Refs. [13–15].

The "external" background corresponds to the "two-electron" events created by γ-rays emitted by the surrounding materials after a radioactive decay or a neutron capture. These photons can interact with the ββ source foils creating "two-electron" events by double Compton scattering, $e^+ e^-$ pair production or a Compton interaction followed by Möller scattering.

3.4. "*One crossing electron*" *events*

To study the external background, the choice of an appropriate channel is needed. Photons of "external background" give Compton electrons in the scintillators which, if produced near the edge, can escape and cross the detector (Fig. 2). These events, called "one crossing electron" (OCE) events, are tagged by TOF measurements. Fig. 3 shows the time difference for all the events with two tracks and fired scintillators recorded by NEMO 2 during

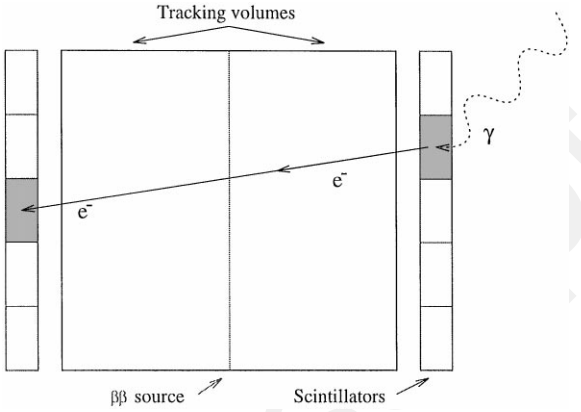

Fig. 2. Scheme of OCE event created by external γ-rays.

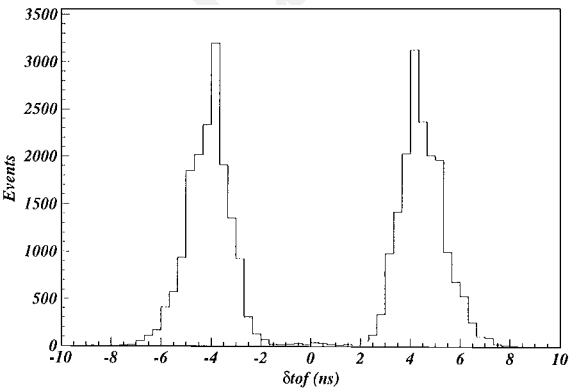

Fig. 3. Distribution of experimental time of flight differences for both "two-electron" events (centered around 0 ns) and OCE events (centered around 4 and − 4 ns) obtained during 10 700 h.

10 700 h of operation. The events coming from the foil ("two electron" events) are centered around 0 ns, while most of the recorded events are OCE events (with a TOF difference of approximately ± 4 ns). Thus, the OCE channel is a good channel to study the external background.

To check the effect of neutrons on this kind of event, data was taken with an Am–Be neutron source placed outside the NEMO 2 prototype shield in two positions. The source was first placed 2 m away from the south wall of the scintillators and then in the plane of the ββ source foil, on the east side. The comparison of the number of OCE events recorded with and without the neutron source (south side) normalized to 1 h is shown in

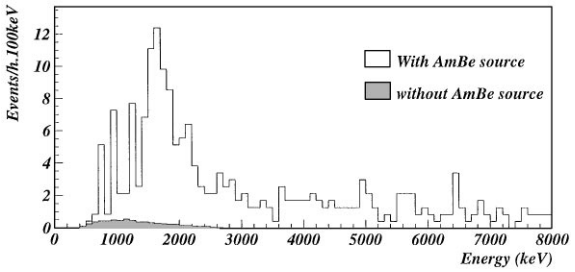

Fig. 4. Energy spectrum of OCE events recorded during 1 h with and without the neutron source with 20 cm iron shield.

Fig. 4. It clearly shows that this channel is sensitive to the neutron contribution. This contribution goes up to 8 MeV (events with one or two saturated counters removed). At this energy events correspond to the interaction of γ-ray from captures in iron and copper frames of the detector. The peak around 1.8 MeV is due to 2.2 MeV γ-rays coming from neutron captures in the hydrogen component of the scintillators.

Note that the detection of neutrons has been previously seen in NEMO 2 data with natural cadmium [12] using the "two-electron" channel and other channels. This provides information on the thermal neutron flux inside the detector. But to measure the contribution of the neutrons to the background, it is needed to measure the γ-ray flux produced by the neutron captures. The OCE events provide information on this γ-ray flux.

4. Simulation of neutron interactions

4.1. Simulation tools

Simulations of neutron interactions were performed with the GEANT/MICAP [16] code which allows one to follow neutrons from 20 MeV down to 10^{-5} eV. The code takes into account γ-ray emission, from (n,γ) captures and (n,n'γ) scatterings. A series of tests were performed with a ^{252}Cf neutron source, a Ge detector and different experimental conditions with several materials like paraffin, iron, copper, lead, etc. The results show that the γ-ray generation subroutines needed to be improved by including additional spectroscopic information related to nuclei. Thus, a new library, GAMLIB, was developed taking into account branching ratios down to 0.1%. Additionally, MICAP was modified to allow for the emission of conversion electrons. This is particularly important for neutron captures with large internal conversion coefficients observed in many nuclei. This was the case in the NEMO 2 data for ^{113}Cd which is present in the natural cadmium ββ source [12].

Table 1
Comparison of simulated and experimental number of events in the OCE channel for 1 h with the Am–Be neutron source located near NEMO 2 in south and east position. Data are is given for two different shields (statistical errors only)

	OCE events per 1 h			
	SOUTH position		EAST position	
	<2.8 MeV	⩾2.8 MeV	<2.8 MeV	⩾2.8 MeV
Iron shield				
Data	105 ± 7	73 ± 6	69 ± 6	55 ± 5
Monte Carlo	128 ± 10	89 ± 9	63 ± 6	44 ± 5
Iron + paraffin shield				
Data	14 ± 3	10 ± 2	8 ± 3	6 ± 2
Monte Carlo	23 ± 7	14 ± 5	6^{+4}_{-2}	13 ± 5

4.2. Data with neutron source

The Am–Be source which was used emitted 6.5×10^4 neutrons s^{-1} (with a mean energy of approximately 5 MeV) and 3.3×10^4 γ-rays s^{-1} at 4.43 MeV from $^{9}\mathrm{Be} + \alpha \rightarrow {}^{13}\mathrm{C}^* \rightarrow {}^{12}\mathrm{C} + \mathrm{n} + \gamma$. In the following, all the simulated data are normalized to these intensities. The neutrons were generated for each source position (as described in Section 3.4) and for two shield configurations (20 cm of iron or 20 cm of iron with 20 cm of paraffin outside of the iron).

Table 1 presents the number of experimental and simulated OCE events for energies greater and lower than 2.8 MeV. The uncertainties correspond only to statistical errors. The systematic errors are estimated at the level of 15% (3% from energy calibration, 10% from the neutron source activity,

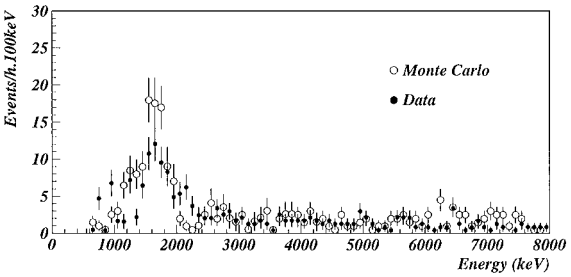

Fig. 5. Comparison of simulated and measured energy spectra of OCE events for one hour with the Am–Be neutron source located on the south side of the NEMO 2 detector.

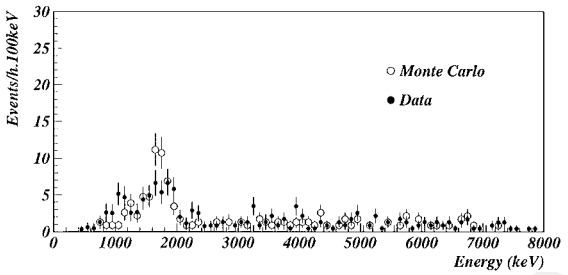

Fig. 6. Comparison of simulated and measured energy spectra of OCE events for 1 h with the Am–Be neutron source located on the east side of the NEMO 2 detector.

10% from the neutron cross-section and 3% from GEANT simulation taken in quadrature). Monte Carlo simulations reproduce the experimental data within 20%.

It can be seen that the reduction factor on the number of events induced by the addition of 20 cm of paraffin is around 10 and is what one expect with such a high-energy neutron source ($\langle E_n \rangle \simeq 5$ MeV).

Figs. 5 and 6 show, in the case of the iron shield, the shape of the measured and simulated OCE spectra. It clearly appears that the experimental spectra are well reproduced by simulations for the two positions of the neutron source.

For all the source and shield configurations discussed above, the observed events are due to the capture of neutrons after thermalization of fast neutrons by elastic scattering in the scintillators. For energies lower than 2.8 MeV most of the events are due to neutron capture in hydrogen contained

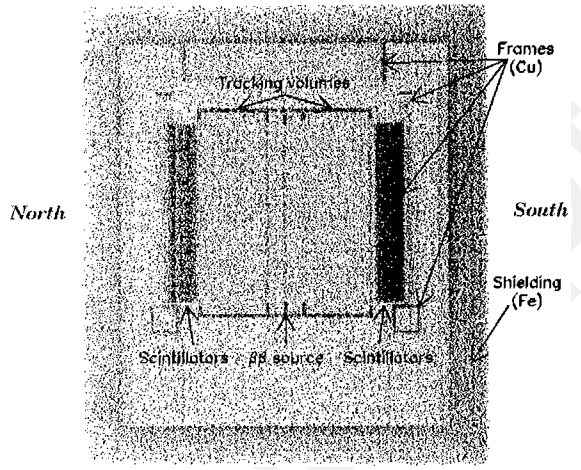

Fig. 7. Projection of the simulated neutron capture places in the NEMO 2 detector in the case of the neutron source located on the south side of the NEMO 2 prototype.

in the scintillators. Above 2.8 MeV γ-rays are produced by neutron capture especially in the copper frames located just behind the scintillator walls as well as in the iron shield. Fig. 7 shows the simulated coordinates of the neutron capture in NEMO 2 detector. The most shaded portions of NEMO 2 correspond to the greatest number of captures. In this figure, the scintillators walls, the inner faces of the iron shield and the different copper frames clearly stand out.

5. Analysis of the recorded OCE events

It is well known that iron absorbs γ-rays and thermal neutrons, lead absorbs γ-rays and paraffin thermalizes fast neutrons and captures thermal neutrons. Several shield configurations were selected to investigate all these effects, firstly 20 cm of iron only, secondly 20 cm of iron and external 5 cm of lead, then 20 cm of iron and internal 5 cm of lead and finally 20 cm of iron and external 20 cm of paraffin. The typical OCE event energy spectrum which was recorded over 10 700 h is given in Fig. 8. The different contributions to the shape of this spectrum are discussed in the following subsections.

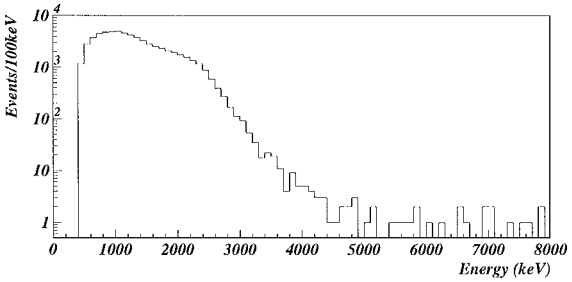

Fig. 8. Energy spectrum of OCE events recorded during 10 700 h (the data of four shield configurations have been added) with the NEMO 2 prototype.

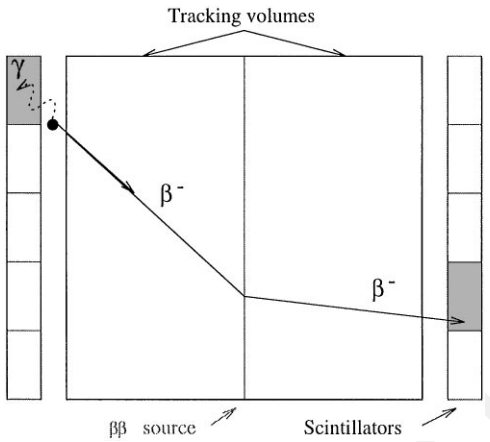

Fig. 9. Scheme of events like OCE events created by ^{208} Tl or ^{214} Bi.

5.1. Bi and Tl components

External ^{214}Bi and ^{208}Tl cannot produce beyond 2.6 MeV OCE-type events such as the one described in Section 3.4. But, for NEMO 2, a β–γ cascade arising from radon and thoron in the air between the calorimeter and the tracking chamber can create events which simulate an OCE event beyond 2.6 MeV (Fig. 9). Moreover, with a contamination of ^{208}Tl ((4 ± 1)Bq m^{-3}) in the scintillator's housing one can produce the same type of events. Our TOF measurement is not robust enough to separate this event topology from the real OCE events (Fig. 2).

The simulation of ^{214}Bi and ^{208}Tl decays (independent of the shield configuration) gives an energy limit on their contribution at 3.2 MeV for bismuth and 4.5 MeV for thallium. The number of expected events per 1000 h given by the simulation is reported in Table 2 assuming activities of (14 ± 4)Bq m^{-3} for radon and (1.3 ± 1.0)Bq m^{-3} for thoron in the LSM. The indicated errors in Table 2 are mainly due to the uncertainties in the measurement of radon, thoron and housing contaminations in the detector. The results show that most of the recorded events below 4.5 MeV are explained by the ^{214}Bi and ^{208}Tl components.

Table 2
Number of simulated OCE events created by ^{208}Tl and ^{214} Bi compared to data normalized to 1000 h. Limits are given at the 90% CL. Uncertainties contain statistical and systematic errors

	OCE events per 1000 h		
	2.8–3.2 MeV	3.2–4.5 MeV	>4.5 MeV
^{214} Bi (radon)	5 ± 2	<0.1	–
^{208} Tl (thoron)	19 ± 15	10 ± 8	<0.02
^{208} Tl (housing)	11 ± 3	3.8 ± 0.9	<0.05
Simulation total	35 ± 15	14 ± 8	<0.07
Data	39 ± 3	13 ± 2	3.2 ± 0.7

5.2. γ-rays from the laboratory

Taking into account the measured γ-ray fluxes given in Section 2.2, simulations have been performed for NEMO 2 for different shield configurations. The results, in the case of the least efficient γ-ray shield of 20 cm of only iron, are summarized in Table 3. All numbers are below 0.3 event per 1000 h beyond 2.8 MeV. This proves that γ-rays coming from the laboratory do not contribute significantly to the OCE channel and consequently to the ββ(0ν) background in the NEMO 2 detector.

5.3. Neutrons from the laboratory

As shown in Section 4.2, neutrons can give events throughout 0–10 MeV energy spectrum and particularly above 4.5 MeV. To understand such events neutron simulations were performed. As the interactions of neutrons depend on their energy, three energy domains for the neutrons were defined to

Table 3
Number of simulated OCE events created by γ-rays produced in the LSM normalized to 1000 h for a 20 cm iron shield. Limits are given at the 90% CL. Uncertainties contain statistical and systematic errors

	OCE events per 1000 h		
γ energy	2.8–3.2 MeV	3.2–4.5 MeV	> 4.5 MeV
3–6 MeV	$(6^{+4}_{-3})\ 10^{-2}$	$(10 \pm 4)\ 10^{-2}$	$(6^{+4}_{-3})\ 10^{-2}$
6–10 MeV	$(3^{+6}_{-2})\ 10^{-2}$	$< 6\ 10^{-2}$	$(16^{+10}_{-6})\ 10^{-2}$
10–32 MeV	$(0.8^{+1.0}_{-0.5})\ 10^{-3}$	$(1.2^{+1.2}_{-0.7})\ 10^{-3}$	$(3^{+2}_{-1})\ 10^{-3}$
Total	$(9^{+7}_{-4})\ 10^{-2}$	$< 24\ 10^{-2}$	$(22^{+11}_{-7})\ 10^{-2}$

distinguish fast (> 1 MeV), thermal (≃ 0.025 eV) and epithermal (≃ 1 eV–1 MeV) neutrons.

5.3.1. Fast neutrons

For fast neutrons, iron behaves like an energy filter. The percentage and the mean energy of neutrons after crossing the iron are quite independent of the initial spectrum. This is due to the anti-resonance in the elastic scattering cross-section of this material. In our case for any incident neutron with energy beyond 1 MeV (region of the last strong anti-resonance), after 20 cm of iron, the neutron energy is on the average 600 keV and the flux is lowered by a factor of five. This means that any incident fast neutron spectrum will lose its characteristic features after 20 cm iron shield leaving a common neutron spectrum. So, for the simulations of fast neutrons from the laboratory the energy distribution of a fission spectrum was used whose average energy is 2 MeV and accords with the measured energy in the LSM. The comparison between simulated OCE events and data is shown in Table 4, for the different shields and energy domains (sensitive and insensitive to ^{214}Bi and ^{208}Tl contributions). Errors on computed neutron contributions are dominated by errors in the measured fast neutron laboratory flux (≃ 25%).

It is clearly seen that fast neutrons can explain the data in the energy range 4.5–8 MeV. From 2.8 to 4.5 MeV only a few events have a neutron origin but, as previously seen, this energy region is dominated by ^{214}Bi and ^{208}Tl contributions.

Table 4
Simulated neutron contribution to OCE events and comparison with data for various shields. Limits are given at 90% CL. Uncertainties in the simulation include statistical and systematic errors

	OCE events per 1000 h	
	2.8–4.5 MeV	4.5–8 MeV
Iron (20 cm) + *internal lead* (5 cm)		
Experimental	52 ± 3	3.2 ± 0.7
Simulated neutron contributions	2 ± 1	6 ± 2
Iron (20 cm) + *external lead* (5 cm)		
Experimental	60 ± 6	5 ± 2
Simulated neutron contributions	4 ± 1	7 ± 3
Iron (20 cm)		
Experimental	64 ± 11	9^{+6}_{-4}
Simulated neutron contributions	3 ± 1	7 ± 3
Iron (20 cm) + external paraffin		
Experimental	48 ± 5	$0.9^{+1.2}_{-0.6}$
Simulated neutron contributions	< 0.1	0.10 ± 0.03

5.3.2. Thermal neutrons

On average the thermal neutrons are captured in the first centimeter of the iron shield ($\lambda \simeq 5$ cm). The remaining thickness of iron is then sufficient to suppress the emitted γ-rays and therefore the OCE events. A simulation leads to a limit (90% CL) of 0.2 OCE events per 1000 h in the high-energy spectrum (2.8–8 MeV). In conclusion, the thermal neutron contribution is negligible in the presence of 20 cm of iron shield.

5.3.3. Epithermal neutrons

As mentioned in Section 2.1 the epithermal neutron flux is on the same level as the thermal neutron flux. Since the energy distribution in the 0.025 eV–1 MeV energy range is not experimentally known, the simulation assumed the same neutron flux for each decade of energy. Fig. 10 shows the number of OCE events (for the full energy range) as a function of these decades of energy. The given number of events are normalized to the fast neutron contribution which is represented by the point at 2 MeV. Below 1 eV only limits (90% CL) have been obtained. The conclusion is that the epithermal

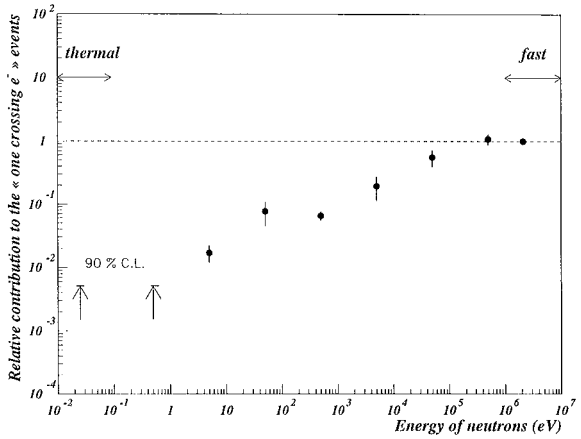

Fig. 10. Contribution of neutrons to the OCE channel as a function of their energy.

Table 5
Summary of experimental and simulated OCE events recorded with various shields. Uncertainties in the simulation contain statistical and systematic errors

	OCE events per 1000 h		
	2.8–3.2 MeV	3.2–4.5 MeV	4.5–8 MeV
Iron (20 cm) + *internal lead* (5 cm)			
Experimental	39 ± 3	13 ± 2	3.2 ± 0.7
Simulation total	35 ± 15	16 ± 8	6 ± 2
Iron (20 cm) + *external lead* (5 cm)			
Experimental	42 ± 5	18 ± 3	5 ± 2
Simulation total	36 ± 15	17 ± 8	7 ± 3
Iron (20 cm)			
Experimental	45 ± 9	19 ± 6	9^{+6}_{-4}
Simulation total	36 ± 15	16 ± 8	7 ± 3
Iron (20 cm) + *external paraffin*			
Experimental	40 ± 4	8 ± 2	$0.9^{+1.2}_{-0.6}$
Simulation total	35 ± 15	14 ± 8	0.10 ± 0.03

neutron cannot be greater than the fast neutron one.

5.4. Discussion

Table 5 summarizes the simulated contributions for each shield and gives a comparison with the corresponding data normalized to 1000 h. To separate the different contributions, data are presented for several energy domains (see Section 5.1).

Taking into account the indicated errors which depend mostly on the measured uncertainties of neutron fluxes and bismuth and thallium activities, it appears that all the considered background sources explain the data for each shield and energy range.

For energies under 4.5 MeV the principle contribution is due to thallium and bismuth given the NEMO 2 geometry (see Section 5.1). Beyond 4.5 MeV all the counting rates are well reproduced by the fast neutron interactions whatever be the shield configuration. This contribution is confirmed by the effect of the additional paraffin shield on the number of OCE events above 4.5 MeV. The estimation of this effect gives an attenuation factor of 70 on the recorded events. This factor is compatible with the data.

5.5. Extrapolation to the background of $\beta\beta(0\nu)$ channel

A similar study has been carried out for the "two-electron" channel. For 10 700 h of data only one "two-electron" event [14] was detected in the energy range of the expected $\beta\beta(0\nu)$ signal (2.8–3.2 MeV). For the same time and the same energy domain, the calculated external background is $(0.6 \pm 0.2)10^{-2}$ events and $(4 \pm 2)10^{-2}$ events from photons and neutrons, respectively. The experimentally observed event is explained by the internal background which predicted 1.2 event from the combination of ^{214}Bi, ^{208}Tl and $\beta\beta(2\nu)$ decays.

Beyond 3.2 MeV, one "two-electron" event was detected. The Monte Carlo calculation for the external background contribution gives an expected number of 1.0 ± 0.4 events coming from neutrons and a limit of 0.7 events (90%) induced by ^{208}Tl from thoron and the scintillator housings.

6. Consequences for the NEMO 3 detector

To reach the expected sensitivity of 0.1 eV for the effective neutrino mass, the NEMO 3 detector must be able to measure $\beta\beta(0\nu)$ half-lives greater than

10^{24} years. This requires the accommodation of 10 kg of enriched ββ source. Simulations show that taking into account the ^{214}Bi and ^{208}Tl activities (for molybdenum these activities are less than 0.3 mBq kg^{-1} and 0.02 mBq kg^{-1} for ^{214}Bi and ^{208}Tl, respectively) and the ββ(2ν) decay, the expected internal background is on the order of two events per year in the energy range 2.8–3.2 MeV.

Therefore, the selected constraint is to have no events (< 0.1) from the external background during the planned five years of data acquisition. Consequently, NEMO 3 has been designed to suppress radon and thoron contaminations and constructed with very severe radiopure selection criteria for its construction materials. Finally, the external background contribution coming from external γ-rays and neutrons will be all eliminated as explained below.

6.1. The NEMO 3 detector

The NEMO 3 detector, as shown in Fig. 11, will be similar in function to the earlier detector, NEMO 2. More specifically, NEMO 3 will also operate in the LSM and will house up to 10 kg of ββ(0ν) decay isotopes. To date, much attention has been focused on 10 k of enriched Mo samples (97% of ^{100}Mo). Also, currently available are the following isotopes: 1 kg of ^{82}Se, 0.6 kg of ^{116}Cd, 0.7 kg of ^{130}Te, 50 g of ^{150}Nd, 16 g of ^{96}Zr and 8 g of ^{48}Ca.

The detector is cylindrical in design and divided into 20 equal sectors. A thin ($\simeq 50$ μm) cylindrical source foil will be constructed from either a metal film or a powder bound by an organic glue to mylar strips. This source will hang between two concentric cylindrical tracking volumes consisting of open octagonal drift cells operating in Geiger mode. These cells run vertically and are staged in a 4, 2, and 3 row pattern to optimize track reconstruction. The optimum design of the drift cells calls for 50 μm stainless-steel anode and cathode wires.

The external walls of these tracking volumes are covered by calorimeters made of large blocks of plastic scintillators coupled to very low radioactivity 3" and 5" Hamamatsu PMTs. The energy resolution depends on the scintillator shape and the associated PMTs. Its range is from 11 to 14.5%

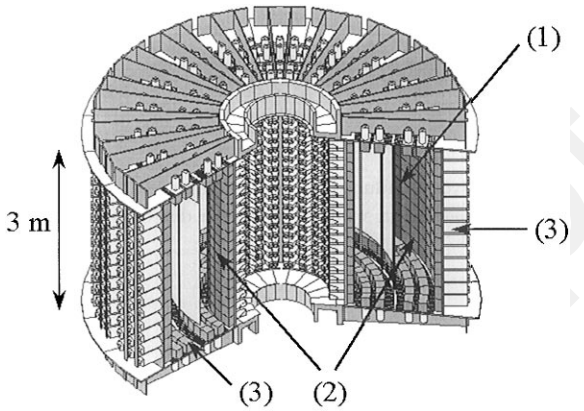

Fig. 11. The NEMO 3 detector. (1) Source foil. (2) Tracking volumes consisting of 3 m vertical Geiger cells. (3) Calorimeter made of plastic scintillators coupled with photomultiplier tubes.

(FWHM) for 1 MeV electrons. Energy and time calibrations will be checked daily by a laser and optical fibers system. The completed detector will contain 6180 drift-Geiger cells and 1940 scintillators.

Cuts on external backgrounds are achieved with a solenoid capable of producing a field of 30 G which will surround the detector to reject (e^+e^-) pair production events. As discussed an external shield in the form of 20 cm of low-activity iron will reduce γ-ray and thermal neutron fluxes. An additional shield will be introduced to suppress the contribution of fast neutrons.

6.2. Selection of events

The selection of events in NEMO 3 is based upon the same principles that were employed in NEMO 2 (see Section 3.2). A charged particle is identified by a track coming from the source foil and depositing its energy in scintillator. Whereas a γ-ray will be identified as a fired scintillator without an associated track [17]. It is also possible to identify alpha particles by short tracks. The TOF calculation is similar to the one in NEMO 2. In addition, NEMO 3 will provide the charge of the particle from the trajectory curvature created by the magnetic field.

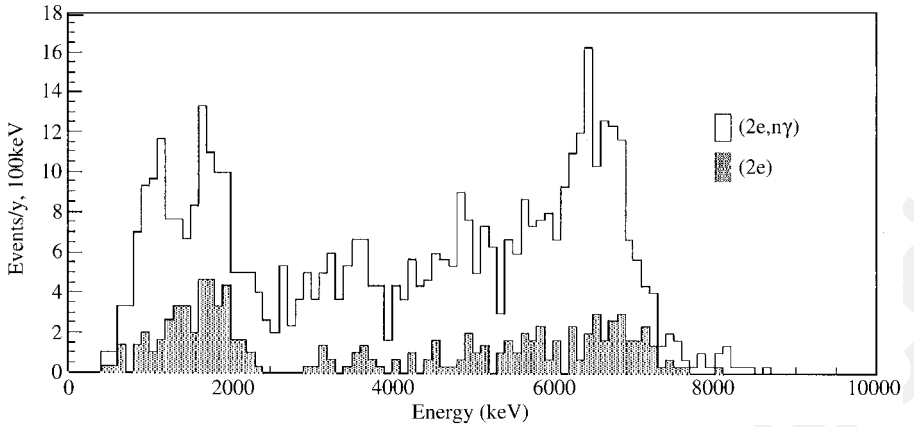

Fig. 12. Simulated "two-electron" events induced by fast neutrons in the NEMO 3 detector for one year of data acquisition. In white events with detected γ-rays, in dark events without detected γ-rays.

6.3. External background

6.3.1. Neutrons

The simulation of the fast neutrons coming from the laboratory in NEMO 3 was done with 20 cm of iron shield. The contribution to the ββ(0ν) background of the photons created by neutron captures leads mainly to (e^+e^-) events and also to a few (e^-e^-) events produced in the source. The near 4π solid-angle coverage of the calorimeter provides a high rejection efficiency (80%) by the detection of the γ-rays associated with the events. This rejection is shown in Fig. 12 which gives the simulated energy spectra of the events with and without detected γ-rays normalized to one year data. The number of events without detected γ-rays is estimated to (260 ± 110) per five years for energies greater than 2.8 MeV (the large uncertainty is due to the large error on the measured fast neutron flux (see Section 2.1)). The magnetic field provides to reject 95% of the (e^+e^-) pairs events. Consequently, the remaining 5% and the (e^-e^-) events give a rate of (50 ± 21) events per five years above 2.8 MeV. These events can be suppressed only if the flux of neutrons inside the detector is decreased. So, a neutron shield consisting of 20 cm of external and 1 cm of internal borated polyethylene (BPE) will be added to the 20 cm iron shield. With this configuration the number of high-energy γ-rays produced by neutron captures inside the detector is reduced by a factor of 100. Note that this shield is optimized to stop fast neutrons with an energy of a few MeV, thus, it also suppress thermal and epithermal neutrons.

Table 6
Simulated neutron background in the "two-electron" channel for five years of data collection and 10 kg of ^{100}Mo for various shields with and without a 30 Gauss magnetic field. Uncertainties contain statistical and systematic errors

	"Two-electron" events per 5 yr	
Shields	>2.8 MeV	2.8–3.2 MeV
Iron (20 cm)	260 ± 110	$10.0^{+7.5}_{-6.0}$
$\vec{B}$ (30 G) and iron (20 cm)	50 ± 21	$1.5^{+4.0}_{-1.2}$
BPE (20 + 1 cm)and iron (20 cm)	2.5 ± 1.0	$0.09^{+0.07}_{-0.06}$
$\vec{B}$ (30 G),BPE (20 + 1 cm) and iron (20 cm)	0.5 ± 0.2	$0.02^{+0.04}_{-0.02}$

Finally, with this shield and the magnetic field, the neutron background is estimated to (0.5 ± 0.2) events for five years above 2.8 MeV. In the energy region of the expected ββ(0ν) signal (2.8–3.2 MeV) the contribution from neutrons is $(0.02^{+0.04}_{-0.02})$ events in five years which is negligible as compared to the 10 expected internal background events [18]. The effects of iron and BPE shields as well as the magnetic field are summarized in Table 6.

Table 7
Estimated γ-ray background in the "two-electron" channel for five years of data collection and 10 kg of ^{100}Mo with various shields with and without a magnetic field. Uncertainties contain statistical and systematic errors

Shields	"Two-electron" events per 5 yr	
	>2.8 MeV	2.8–3.2 MeV
Iron (20 cm)	26 ± 8	1.0 ± 0.3
$\vec{B}$ (30 G) and iron (20 cm)	5.0 ± 1.5	0.15 ± 0.05
BPE (20 + 1 cm) and iron (20 cm)	13 ± 4	0.5 ± 0.2
$\vec{B}$ (30 G), BPE (20 + 1 cm) and iron (20 cm)	2.5 ± 0.8	0.10 ± 0.03

6.3.2. γ-rays

Shown in Section 5.2 is the background induced by the γ-rays coming from the laboratory which was 10 times less than the background due to neutrons. But, in NEMO 3, the paraffin shield decreases the γ-ray fluxes by just a factor of two compared to the factor of 100 obtained for the neutrons. Taking into account the uncertainties on the γ-ray fluxes this background is estimated in NEMO 3 at (2.5 ± 0.8) events above 2.8 MeV of which (0.10 ± 0.03) event between 2.8 and 3.2 MeV for the five years of data acquisition. The estimated γ-ray contribution in terms of the shields are summarized in Table 7.

7. Conclusion

The NEMO 2 prototype provided a useful study of the backgrounds for the ββ(0ν) decay induced by γ-rays and neutrons coming from the laboratory. Various shields and measurements with a neutron source have been used to identify the different components. To compare data and Monte Carlo calculations, this study requires the development of an interface between GEANT/MICAP and a new library for γ-rays emission after capture or inelastic scattering of neutrons.

This study of the neutrons inside the detector has shown that the dominant background at high energies is fast neutrons from the laboratory. With an appropriate neutron shield and a magnetic field, the NEMO 3 experiment can be liberated from the neutron background. The magnetic field also effectively reduces the γ-ray background in the ββ(0ν) energy window.

Acknowledgements

The authors would like to thank the Fréjus underground laboratory staff for their technical assistance in running the experiment.

References

[1] M. Doi, T. Kotani, E. Takasugi, Prog. Theor. Phys. (Suppl.) 83 (1985) 1.
[2] S.M. Bilenki et al., Phys. Lett. B 465 (1999) 198.
[3] D. Dassié et al., Nucl. Instr. and Meth. A 309 (1991) 465.
[4] R. Arnold et al., Nucl. Instr. and Meth. A 354 (1995) 338.
[5] NEMO-3 proposal. LAL preprint 94-29, 1994.
[6] A. Rindi et al., Nucl. Instr. and Meth. A 272 (1988) 871.
[7] V. Chazal et al., Astropart. and Phys. 9 (1998) 163.
[8] G.T. Ewan, Nucl. Instr. and Meth. A 314 (1992) 373.
[9] S.R. HXSashemi-Nezhad, L.S. Peak, Nucl. Instr. and Meth. A 357 (1995) 524.
[10] Ph. Hubert, I. Ohsumi, NEMO meeting Report, 1999.
[11] D. Dassié et al., Phys. Rev. D 51 (1995) 2090.
[12] R. Arnold et al., Z. Phys. C 72 (1996) 239.
[13] R. Arnold et al., Nucl. Instr. and Meth. A 401 (1997) 144.
[14] R. Arnold et al., Nucl. Phys. A 636 (1998) 209.
[15] R. Arnold et al., Nucl. Phys. A 658 (1999) 299.
[16] C. Zeitnitz, T.A. Gabriel, Nucl. Instr. and Meth. A 349 (1994) 106.
[17] I. Kisel et al., Nucl. Instr. and Meth. A 387 (1997) 433.
[18] F. Piquemal for the NEMO collaboration, Proceedings of the XVIII International Conference on Neutrino Physics and Astrophysics, Takayama, Japan, 4–9 June 1998; Nucl. Phys. B 77 (1999) 352.